Multiphase-Field Simulation of Cementite Precipitation during Isothermal Lower Bainitic Transformation

Wenwen Song, Ulrich Prahl, Yan Ma, and Wolfgang Bleck*

In the present work, isothermal lower bainitic transformation with nano-sized cementite (θ) precipitation is simulated by means of multiphase-field approach. In order to simulate the very fine cementite, ultra-small grid spacing, that is, 2 nm, is applied. A faceted anisotropy model is coupled in the simulation of both bainitic ferrite (α_B) and cementite (θ) growth. The simulated microstructure evolution and bainite fraction are compared with experimental results. Carbon redistribution across γ/α_B and α_B/θ phase boundaries during lower bainitic transformation is further discussed.

Bainitic steels are widely applied in the manufacturing, automotive, and construction industry. The sophisticated bainitic microstructure provides bainitic steels with a combination of high strength and good toughness.[1] A considerable amount of research work has been carried out to understand the bainitic transformation over many decades,[2–10] since its discovery in 1930.[11] The bainitic microstructure can be designated to upper bainite and lower bainite in medium- and high-carbon steels.[12] Both the upper bainite and lower bainite consist of bainitic ferrite and cementite. The quantitative description of bainite morphology and bainitic transformation kinetics is of great significance for the heat treatment adjustment and mechanical property control of bainitic steels.

Phase-field method is a powerful tool in the visualization of microstructure evolution during distinct phase transformations in material simulations.[13–15] Over the last two decades, the phase-field approach has been increasingly employed in a variety of applications, for example, solidification,[16] solid phase transformation,[17–24] recrystallization,[25,26] segregation behavior,[27] etc. The austenite formation[28–30] and most of the austenite decomposition reactions, for example, ferrite formation,[17–19] pearlite formation,[20,21] martensite formation,[22,23] have been extensively studied using phase-field method, albeit with an exception of bainite formation. In the recent years, dedicated single phase-field models were developed assuming displacive bainitic phase transformation by Arif and Qin,[31] and Düsing and Mahnken,[32] respectively. Zhang et al.[18] reported that accounting for anisotropic elastic energy is sufficient to simulate the formation of Widmanstätten ferrite with their phase-field modeling. Notable progress of bainite simulation work has been developed by Toloui and Militzer[33] using multiphase-field approach to simulate the carbide-free bainite formation in TRIP steel.

Due to the complexity of bainitic transformation mechanisms, phase-field simulation of bainite formation still remains a challenge. On the one hand, the bainitic transformation shows the coupled diffusive-mechanical mechanisms, which requires either complex coupled models or a diffusion-driven model, that is, only valid for specific situations. On the other hand, the two-scale nature of bainite, that is, bainitic sheaves in micrometer scale and carbides in nanometer scale, needs either a two-scale approach or very tiny grid size. In most of the phase-field models for bainitic transformation in literature, either bainite was considered as ferrite or only carbide-free bainite was considered. So far, the carbide precipitation has been long-term neglected in the phase-field simulation of bainitic transformation.

In the present work, both bainitic ferrite (α_B) formation and nano-sized cementite (θ) precipitation during isothermal lower bainitic transformation are simulated by a multiphase-field approach, employing a faceted anisotropy model. The diffusion (chemical) effects during bainitic transformation are considered in a physical way by solving the multiphase-field functions. In addition, the mechanical contribution of bainitic phase transformation is simulated by employing the "faceted growth" model. A 2-dimensional phase-field simulation with an ultra-small grid spacing, that is, 2 nm, is performed using the commercial software MICRESS® (MICRostructure Evolution Simulation Software).[35] The simulated microstructure evolution and bainite fraction are compared with experimental results. Carbon redistribution across γ/α_B and α_B/θ phase boundaries during lower bainitic transformation is investigated and further discussed.

1. Experimental Section

The chemical composition of the studied material 100Cr6 is Fe–0.967C–0.3Si–0.23Mn–1.38Cr (wt%). After hot forging, the material was soft annealed at 800 °C followed by a slow cooling to room temperature. Subsequently, the samples were heated up at a rate of 3.3 °C s^{-1} and austenitized at 910 °C for 3600 s, followed

W. W. Song, Y. Ma, Prof. W. G. Bleck
Steel Institute
RWTH Aachen University
Intzestr. 1, 52072 Aachen, Germany
E-mail: wenwen.song@iehk.rwth-aachen.de

Prof. U. Prahl
Institut für Metallformung
TU Bergakademie Freiberg
Bernhard-von-Cotta-Str. 4, 09599 Freiberg, Germany

The ORCID identification number(s) for the author(s) of this article can be found under https://doi.org/10.1002/srin.201800028.

DOI: 10.1002/srin.201800028

by rapid cooling to 260 °C at a cooling rate of 55 °C s^{-1}. At the isothermal bainitic transformation temperature of 260 °C, the samples were held for 1500 s followed by a rapid cooling to room temperature. Austenitization and bainitization were performed in a Bähr 805A dilatometer. Specimen dimensions were 3 mm in diameter and 10 mm in length. In addition, the phase fraction was determined by the metallography approach using Zeiss Sigma field emission scanning electron microscope (SEM). The SEM samples were mechanically ground, polished and then etched with nital-3% (HNO_3). The bainite fraction was estimated from the area fraction in the SEM images by contrast analysis based on its needle-shaped morphology using ImageJ software. The bainite fraction (f_B) was calculated by the following equation:

$$f_B = \sum A_{Bi}/A_{image} \tag{1}$$

where, A_{Bi} is the area of single bainite needle and A_{image} is the area of SEM image. With an extra low scanning voltage (about 2 keV), close working distance, high contrast, and slow scanning speed, the in-lens detector allowed us to identify clearly the bainitic needle-shape morphology. In order to achieve reasonable statistics, six SEM images in dimensions of 18 μm × 18 μm were selected under each heat treatment conditions for bainite fraction measurement.

2. Phase-Field Simulation

The multiphase-field model proposed by Steinbach et al.[36] is applied in the present work to simulate isothermal bainitic transformation at 260 °C in 100Cr6. The transformation kinetics is described by phase-field parameters $\phi_i (i = 1 \ldots N)$. ϕ_i assumes a value of 1 inside grain i and 0 outside of the grain. At the interface between two grains i and j, $0 < \phi_i < 1$, $0 < \phi_j < 1$, and $\phi_i + \phi_j = 1$. In general, $\sum_i^N \phi_i(r,t) = 1$ holds at each position r in the simulation domain with a total number of N grains. In the case of a double-well potential, the change rate of each phase-field parameter with time is given by pairwise interactions with neighboring grains[36]:

$$\frac{d\phi_i}{dt} = \sum_j \mu_{ij}\left[\sigma_{ij}\left(\phi_i\nabla^2\phi_j - \phi_j\nabla^2\phi_i + \frac{\pi^2}{2\eta_{ij}^2}\left(\phi_i - \phi_j\right)\right) + \frac{\pi}{\eta_{ij}}\sqrt{\phi_i\phi_j\Delta G_{ij}}\right] \tag{2}$$

where, η, σ_{ij}, μ_{ij}, and ΔG_{ij} represent interface width, surface energy, interface mobility, and free energy difference of two interacting grains or phases i and j, respectively. The first term of Equation (2) represents the interface curvature and the second term stands for the thermodynamic driving force. The driving force ΔG_{ij} is assumed to be proportional to the local undercooling ΔT, as given by Equation (3)[37]:

$$\Delta G_{ij} = \Delta S_{ij}\Delta T = \Delta S_{ij}(T^{eq} - T) \tag{3}$$

where, ΔS_{ij} value links the undercooling and the driving pressure during the phase transformation, and T^{eq} represents the local equilibrium temperature.

Carbon fluxes are calculated from the composition gradient and the diffusivity in each grain. The time dependence of the local concentration of carbon in a phase is given by:

$$\frac{\partial c}{\partial t} = \nabla \cdot \sum \phi_i D_i \nabla c_i \tag{4}$$

where, c_i is the carbon concentration and D_i represents the diffusivity in phase i.

The austenite (γ) was assumed to be isotropic, which decomposes into bainite identically in all directions. To describe the anisotropic growth of α_B and θ according to their morphologies, a faceted anisotropy model[34] implemented in MICRESS® was applied. In this model, it is assumed that each crystallographic orientation has individual properties, for example, interfacial energy and interfacial mobility.[34] For each facet type, the interfacial energy is calculated as:

$$\sigma = \sigma_0 \cdot k_{st}^2 \cdot \left(k_{st}^2 \cdot \cos\beta^2 + \sin\beta^2\right)^{-\frac{3}{2}} \tag{5}$$

where, σ_0 is the interfacial energy coefficient between two phases, k_{st} is the static anisotropy coefficient of the facet, and β is the misorientation of the normal vector of the interface to the normal vector of the nearest facet. The interfacial mobility is calculated as the following equation:

$$\mu = \mu_0\left[k_{kin} + (1 - k_{kin}) \cdot \tan\left(\frac{\kappa}{\tan\beta}\right) \cdot \frac{\tan\beta}{\kappa}\right] \tag{6}$$

where, μ_0 is the interfacial kinetic coefficient between two phases, indicating the interface mobility; k_{kin} is the kinetic anisotropy coefficient; the κ value defines the broadness of anisotropy with the value in the range of 0 and 1. The static anisotropy coefficient (k_{st}) and the kinetic anisotropy coefficient (k_{kin}) describe the anisotropy characteristics of the bainite and cementite growth. A smaller kinetic anisotropy coefficient indicates a higher degree of anisotropy. $k_{kin} = 1$ indicates the isotropic growth and $k_{kin} = 0$ indicates the maximal anisotropic growth. A smaller k_{kin} illustrates a faster interface mobility decrease, thus leads to a larger lengthening rate and sharper growth tip. For replicating the experimental microstructural observation, $\kappa = 0.95$, $k_{st} = 3 \times 10^{-3}$, and $k_{kin} = 8 \times 10^{-3}$ were used in the simulation of bainite transformation.

The size of the domain was 2 μm × 8 μm. An ultra-small grid spacing $\Delta X = 2$ nm has been applied in order to resolve very fine cementite within the bainitic structure. The thickness of an interface between the phases was defined to be five times of the grid spacing, that is, $\eta = 5\Delta X$. In the phase-field simulation, carbon was assumed to be homogeneously distributed with the nominal concentration in the initial γ grain. θ carbide was considered to nucleate within α_B bulk or at α_B/γ boundaries, whereas θ precipitation from γ was not included in the model. α_B was assumed to be randomly distributed in the austenite bulk area, maintaining a Kurdjumov-Sachs (KS) crystallo graphic orientation relationship with the γ. The orientation angle between bainite and austenite was assigned in the simulation in respect with the orientation relationship between bainite and austenite, however, the actual K-S orientation

Table 1. Input interface and diffusion parameters in phase-field simulation of lower bainitic transformation in 100Cr6.

Parameters		Values	Ref.
Interface properties	Interfacial energy coefficient σ_0	2.0E–05 J/cm^{-2} (All interfaces)	[39]
	γ/α_B interfacial kinetic coefficient μ_0^{γ/α_B}	3.0E-09 cm$^4 \cdot$ J$^{-1} \cdot$ s^{-1}	–
	α_B/θ interfacial kinetic coefficient $\mu_0^{\alpha_B/\theta}$	1.0E-11 cm$^4 \cdot$ J$^{-1} \cdot$ s^{-1}	–
Diffusion data	Pre-exponential term of the C diffusion coefficient in austenite D_{0C}^{γ}	0.15 cm$^2 \cdot$ s^{-1}	[21]
	Pre-exponential term of the C diffusion coefficient in ferrite D_{0C}^{α}	2.2 cm$^2 \cdot$ s^{-1}	[21]
	Activation energy for carbon diffusion in austenite Q_C^{γ}	1.421E + 05 J $\cdot$ mol^{-1}	[21]
	Activation energy for carbon diffusion in ferrite Q_C^{α}	1.225E + 05 J $\cdot$ mol^{-1}	[21]

relationship was not represented. The simulation was conducted with periodic boundary conditions. Three phases were involved in the simulation of austenite decomposition and bainite formation process: γ, α_B, and θ. θ was considered as stoichiometric with a constant carbon concentration of 6.67 wt%.

The thermodynamic interactions between phases were described by a linearized para-equilibrium phase diagram, which was calculated using Thermo-Calc software with the TCFe7 database based on CALPHAD (CALculation of PHAse Diagrams) method. The thermodynamic interactions between the phases, that is, austenite (γ), bainitic ferrite (α_B), and cementite (θ), were defined on the basis of a para-equilibrium phase diagram, assuming that only carbon redistributes via diffusion, whereas substitutional alloy elements such as Cr, Mn, and Si, are considered to be frozen-in. $x_C^{\alpha_B/\gamma}$ and x_C^{γ/α_B} are the respective carbon concentrations in the bainitic ferrite (α_B) and in the austenite (γ) during bainitic ferrite formation ($\gamma \rightarrow \alpha_B$). $x_C^{\alpha_B/\theta}$ and x_C^{θ/α_B} are the respective carbon concentrations in bainitic ferrite (α_B) and cementite (θ) during cementite (θ) precipitation ($\alpha_B \rightarrow \theta$). Our previous investigation by atom probe tomography (APT) revealed that the θ precipitates form under para-equilibrium mode and the carbon partially partitions between γ and α_B during $\gamma \rightarrow \alpha_B$ transformation.[38] The carbon diffusivities in α_B and γ were calculated according to the Arrhenius equation $D = D_0 \exp(-Q_D/RT)$. The input interface and diffusion parameters applied for the phase-field simulation of bainitic transformation are listed in **Table 1**. The interfacial

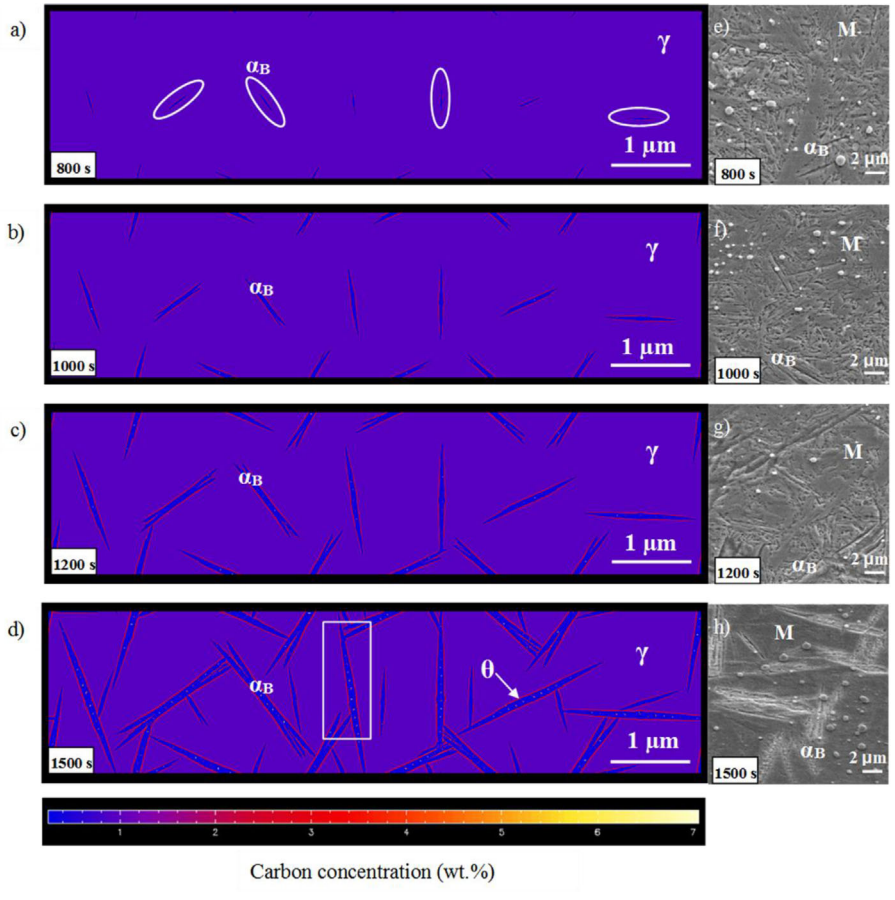

Figure 1. Evolution of carbon concentration in the simulated bainite microstructure during isothermal lower bainitic transformation in 100Cr6 steel at 260 °C for a) 800 s, b) 1000 s, c) 1200 s, and d) 1500 s; Corresponding SEM micrographs e) 800 s, f) 1000 s, g) 1200 s, and h) 1500 s. γ: austenite; α_B: bainitic ferrite; θ: cementite; M represents martensite, which is formed from austenite during quenching in experiment.[38]

kinetic coefficient parameters in this study were used as fit parameters, in order to replicate the experimental observations.

3. Results and Discussion

3.1. Microstructure Evolution during Bainite Formation

Figure 1 displays the simulated carbon concentration evolution during isothermal bainitic transformation at 260 °C in the high-carbon steel 100Cr6. The initial bainite plate nucleation and growth sites are indicated and marked with white ellipses. The bainitic ferrite (α_B) nucleates randomly in the austenite (γ) matrix. During bainitic transformation, the bainite plates grow with a rapid lengthening rate at the early stage followed by thickening and cementite (θ) precipitation. The simulated microstructure (Figure 1a–d) shows a good agreement with bainite microstructure observed in the SEM micrographs (Figure 1e–h). During bainitic transformation, the excess carbon within α_B partitions into γ, which leads to a higher carbon concentration in γ at α_B/γ phase boundaries. This is indicated by the color change of γ in the simulation in Figure 1a–d.

3.2. Carbon Redistribution across Phase Boundaries during Bainite Formation

Figure 2 shows the simulated θ precipitation in a single lower bainite plate after isothermal bainitic transformation at 260 °C for 1500 s. Figure 2a corresponds to the selected region of interest in the white rectangular in the simulated microstructure in Figure 1d. In Figure 2a, θprecipitates at an inclination of about 60° with respect to the long axis of α_B, which was predefined in the simulation according to the morphological characteristics of bainite microstructure in the transmission electron microscopy (TEM) bright field image.[40] It was reported that the carbide precipitation within bainitic structure tends to adopt a single crystallographic variant in an α_B plate and this is different from the carbide precipitation in tempered martensite with multiple

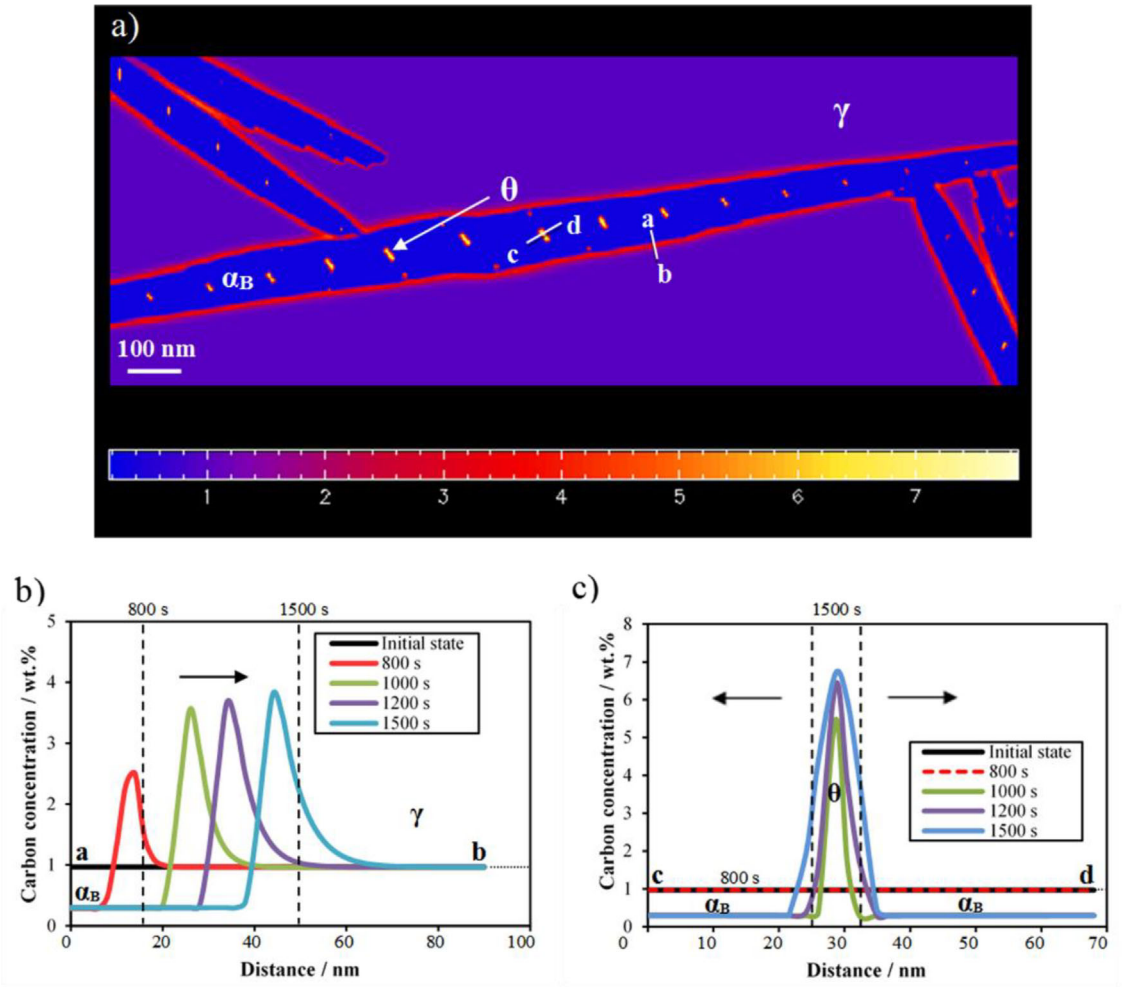

Figure 2. a) The simulated bainite microstructure after isothermal lower bainitic transformation at 260 °C for 1500 s and the domain corresponds to the selected region of interest in Figure 1d; b) carbon concentration along the a-b line in a) across γ/α_B phase boundary; c) carbon concentration along the c-d line in a) across α_B/θ phase boundary.[38]

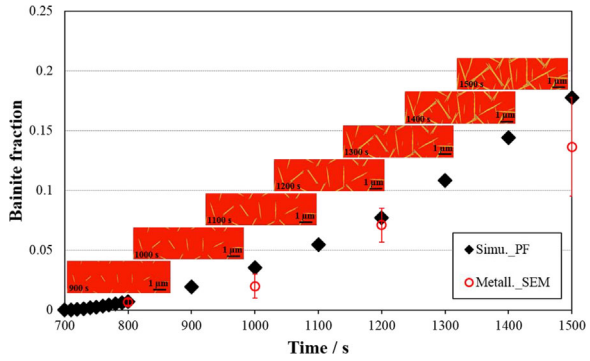

Figure 3. Simulated bainite fraction in 100Cr6 during isothermal bainitic transformation at 260 °C and experimentally determined bainite fraction by metallographic analysis. In the simulated microstructure, red phase represents austenite, yellow phase represents bainitic ferrite, and white phase represents cementite.[38]

crystallographic variants.[41] The angle quoted in carbide precipitation within the bainitic structure varies as a function of the plane of section. For the α_B with a habit plane $(0.761\ 0.169\ 0.626)_\gamma$, θ precipitates on $(1\bar{1}2)_\alpha$ maintaining an angle of 57° between α_B and θ habit plane normal.[1,40]

Figure 2b illustrates the carbon concentration profiles along the a-b line in Figure 2a, showing the migrating α_B/γ phase boundary and carbon redistribution behavior during α_B thickening at 260 °C. The simulated α_B formation is accompanied by carbon diffusion from the α_B to γ, while substitutional elements, that is, Cr, Si, Mn, are frozen in the sublattice. This agrees well with previous APT analysis.[38] Figure 2c illustrates carbon concentration along the c-d line in Figure 2a, showing the migrating α_B/θ phase boundary and carbon redistribution across the phase boundary during θ precipitation. θ nucleates and precipitates from the α_B plate when the minimum local undercooling in α_B is achieved for θ formation. Carbon is near-equilibrated under para-equilibrium mode during the θ precipitation within α_B.

3.3. Comparison of Simulated and Experimental Transformation Kinetics during Bainite Formation

Figure 3 manifests the simulated microstructure evolution in 100Cr6 during isothermal bainitic transformation at 260 °C and the α_B volume fraction as a function of isothermal bainitic transformation time. The red phase in Figure 3 represents austenite, yellow phase represents bainitic ferrite and white phase stands for cementite. The simulation shows that the bainite fraction increases progressively with an increase in the bainitic transformation time after the incubation period. The bainite fraction achieves approximately 0.18 after bainitic transformation at 260 °C for 1500 s. The simulated bainite fraction (Simu._PF) is compared with the metallographic approach determined bainite fraction (Metall._SEM) in 100Cr6. The experimental and phase-field simulated kinetics agree well with a deviation of about 0.02 in bainite fraction. The metallographic approach evaluates the area fraction of different phases in a cross section (in two dimensions), which might lead to a slight underestimation of bainite fraction. The bainitic transformation kinetics is strongly affected by the kinetic parameters in the simulation, that is, diffusivity, interfacial mobility etc. Therefore, the appropriate kinetic data input is crucial in the further application of the present model for simulating θ precipitation during lower bainitic transformation. In particular, in the cases which bainitic transformation kinetics are influenced by, for example, different alloy concepts, different heat treatment conditions, proper kinetics data should be considered.

4. Conclusions and Outlook

In the present work, a phase-field model was proposed for simulating nano-sized cementite (θ) precipitation during isothermal lower bainitic transformation. The simulated microstructure evolution by phase-field modeling was compared with SEM data. As the very first attempt to simulate *θ* precipitation during lower bainitic transformation, the phase-field simulated results and the experimental analysis showed good agreement. Phase-field simulation coupled with the faceted anisotropy model seems to be a promising tool in material simulations, particularly for the complex bainitic transformation.

Acknowledgements

This work was performed within the Interdisciplinary Centre for Advanced Materials Simulation (ICAMS) at Ruhr University Bochum. The authors gratefully acknowledge Prof. Ingo Steinbach at Ruhr University Bochum, Dr. Markus Apel and Dr. Janin Eiken at ACCESS e.V. for the helpful discussions.

Conflict of Interest

The authors declare no conflict of interest.

Keywords

bainite, cementite precipitation, phase-field simulation

Received: January 16, 2018
Revised: May 25, 2018
Published online:

[1] H. K. D. H. Bhadeshia, J. W. Christian, *Metall. Trans. A* **1990**, *21*, 767.
[2] M. Hillert, *Jernkontorets Annaler* **1957**, *141*, 757.
[3] H. K. D. H. Bhadeshia, D. V. Edmonds, *Metall. Trans. A* **1979**, *10*, 895.
[4] H. K. D. H. Bhadeshia, A. R. Waugh, *Acta Metall.* **1982**, *30*, 775.
[5] M. Hillert, *Metall. Mater. Trans. A* **1994**, *25*, 1957.
[6] A. Borgenstam, M. Hillert, J. Ågren, *Acta Mater.* **2009**, *57*, 3242.
[7] E. V. Pereloma, *Mater. Sci. Technol.* **2016**, *32*, 99.
[8] C. Garcia-Mateo, J. A. Jimenez, H.-W. Yen, M. K. Miller, L. Morales-Rivas, M. Kuntz, S. P. Ringer, J.-R. Yang, F. G. Caballero, *Acta Mater.* **2015**, *91*, 162.

[9] Y. Xia, G. Miyamoto, Z. G. Yang, C. Zhang, T. Furuhara, *Acta Mater.* **2015**, *91*, 10.
[10] F. G. Caballero, M. K. Miller, C. Garcia-Mateo, J. Cornide, *J. Alloys Compd*. **2013**, *577*, 626.
[11] E. S. Davenport, E. C. Bain, *TMS-AIME* **1930**, *90*, 117.
[12] R. F. Mehl, in *Hardenability of Alloy Steels*, Symposium Amer. Soc. Met., Cleveland **1939**, p. 1.
[13] I. Steinbach, *Modell. Simul. Mater. Sci. Eng*. **2009**, *17*, 73001.
[14] I. Singer-Loginova, H. M. Singer, *Rep. Prog. Phys*. **2008**, *71*, 106501.
[15] M. Militzer, *Curr. Opin. Solid State Mater. Sci*. **2011**, *15*, 106.
[16] J. Rezende, R. Siquieri, H. Emmerich, A. Lob, D. Senk, D. Djurovic, B. Hallstedt, S. Richter, J. Mayer, *Steel Res. Int*. **2009**, *80*, 609.
[17] M. G. Mecozzi, J. Sietsma, S. van der Zwaag, M. Apel, P. Schaffnit, I. Steinbach, *Metall. Mater. Trans A* **2005**, *36*, 2327.
[18] L. Zhang, Y. Shen, H. Wan, X. Xiong, L. Zhang, *J. Alloys Compd*. **2015**, *650*, 239.
[19] G. Pariser, P. Schaffnit, I. Steinbach, W. Bleck, *Steel Res*. **2001**, *72*, 354.
[20] K. Nakajima, M. Apel, I. Steinbach, *Acta Mater.* **2006**, *54*, 3665.
[21] I. Steinbach, M. Apel, *Acta Mater.* **2007**, *55*, 4817.
[22] E. Borukhovich, G. Du, M. Stratmann, M. Boeff, O. Shchyglo, A. Hartmaier, I. Steinbach, *Materials* **2016**, *9*, 673.
[23] H. K. Yeddu, A. Malik, J. Ågren, G. Amberg, A. Borgenstam, *Acta Mater.* **2012**, *60*, 1538.
[24] M. G. Mecozzi, J. Eiken, M. J. Santofimia, J. Sietsma, *Comput. Mater. Sci*. **2016**, *112*, 245.
[25] O. Güvenç, M. Bambach, G. Hirt, *Steel Res. Int*. **2014**, *85*, 999.
[26] B. Zhu, M. MILITZER, *Modell. Simul. Mater. Sci. Eng*. **2012**, *20*, 85011.
[27] M. Maalekian, H. Azizi-Alizamini, M. Militzer, *Metall. Mater. Trans. A* **2016**, *47*, 608.
[28] M. Militzer, H. Azizi-Alizamini, *Solid State Phenom*. **2011**, *172–174*, 1050.
[29] J. Rudnizki, B. Böttger, U. Prahl, W. Bleck, *Metall. Mater. Trans. A* **2011**, *42*, 2516.
[30] B. Zhu, M. Militzer, *Metall. Mater. Trans. A* **2015**, *46*, 1073.
[31] T. T. Arif, R. S. Qin, *Comput. Mater. Sci*. **2013**, *77*, 230.
[32] M. Düsing, R. Mahnken, *Arch. Appl. Mech*. **2016**, *86*, 1947.
[33] M. Toloui, M. Militzer, *Acta Mater.* **2018**, *144*, 786.
[34] I. Steinbach, F. Pezzolla, R. Prieler, in *Modeling of Casting, Welding, and Advanced Solidification Processes VII Proceedings of the Seventh Conference in a Series on Modeling, Casting, and Welding Processes, Held in London, England from 10–15 September 1995* (Eds: M. Cross, J. Campbell), Minerals, Metals & Materials Society, Warrendale, PA **1995**, p. 695.
[35] *MICRESS*® (Internet), cited June 17, 2018, Available from: http://web.micress.de
[36] I. Steinbach, F. Pezzolla, B. Nestler, M. Seeßelberg, R. Prieler, G. J. Schmitz, J. Rezende, *Phys. D* **1996**, *94*, 135.
[37] J. Tiaden, B. Nestler, H. J. Diepers, I. Steinbach, *Phys. D: Nonlinear Phenom*. **1998**, *115*, 73.
[38] W. Song, *Characterization and Simulation of Bainite Transformation in High Carbon Bearing Steel 100Cr6*, Ph.D. Dissertation, RWTH Aachen University, Aachen **2014**.
[39] N. V. Luzginova, L. Zhao, J. Sietsma, *Mater. Sci. Eng. A* **2008**, *481–482*, 766.
[40] W. Song, J. von Appen, P. Choi, R. Dronskowski, D. Raabe, W. Bleck, *Acta Mater.* **2013**, *61*, 7582.
[41] G. Y. Lai, *Metall. Trans. A* **1975**, *6*, 1469.

